X-ray photoelectron diffraction analysis of the epitaxial growth of titanium on the (110) surface of aluminum
by Volker Krasemann

A thesis submitted in partial fulfillment of the requirements of the degree of Master of Science in Physics
Montana State University
© Copyright by Volker Krasemann (1996)

Abstract:
The growth of Ti films on the Al(110) surface at room temperature has been studied using X-ray photoelectron diffraction (XPD) and low energy electron diffraction (LEED). The overlayer coverages were determined with RBS. The area under the Al 2p and the Ti 2p| 1/2 and 2p 3/2 photoelectron peaks was recorded in dependence of the polar angle.

Both LEED and XPD support an epitaxial growth of Ti on Al in form of islands. The structure of the Ti overlayer is pseudomorphic fee. A distortion of the overlayer was measured with LEED. The interlayer distance of the first two Ti overlayer is smaller than that for the bulk Al as can be concluded from a shift of the forwardscattering peak in the diffraction pattern for Ti.

A shift of the forward-scattering peak in the polar angle scan for Al indicates an expansion of the first. top layers in the Al substrate. Due to the absence of a strong forward-scattering peak in the Al scan for coverages above three monolayers the interdiffusion of bulk Al into the Ti film can be ruled out.

The Ti overlayer exhibits no long-range order for coverages of eight monolayers but still shows short-range order according to XPD.

X-RAY PHOTOELECTRON DIFFRACTION ANALYSIS OF THE EPITAXIAL GROWTH OF TITANIUM ON THE (110) SURFACE OF ALUMINUM

by

Volker Krasemann

A thesis submitted in partial fulfillment

of the requirements of the degree

of

Master of Science

in

Physics

MONTANA STATE UNIVERSITY-BOZEMAN
Bozeman, Montana

June, 1996

N378
K8648

APPROVAL

of a thesis submitted by

Volker Krasemann

This thesis has been read by each member of the thesis committee, and has been found to be satisfactory regarding content, English usage, format, citations, bibliographic style, and consistency, and is ready for submission to the College of Graduate Studies.

7-12-96 R. J. Smith

Date Chairperson, Graduate Committee

Approved for the Physics Department

7-12-96

Date Head, Physics Department

Approved for the College of Graduate Studies

7/30/96

Date Graduate Dean

STATEMENT OF PERMISSION TO USE

In presenting this thesis in partial fulfillment of the requirements for a master's degree at Montana State University - Bozeman, I agree that the Library shall make it available to borrowers under rules of the Library.

If I have indicated my intention to copyright this thesis by including a copyright notice page, copying is allowable only for scholarly purposes, consistent with "fair use" as prescribed in the U.S. Copyright Law. Requests for permission for extended quotation from or reproduction of this thesis in whole or in parts may be granted only by the copyright holder.

Signature

Date 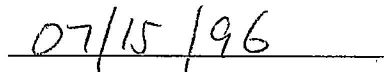

I wish to dedicate this thesis to

David Letterman

ACKNOWLEDGMENTS

I wish to acknowledge Dr. Richard J. Smith to whom I am very thankful for his advice and guidance and for all his support not only in regards to this thesis. It was a great pleasure to be a student under Dr. Smith's supervision. I am thankful to the Physics Department, especially Dr. J. C. Hermanson for the help and financial support I received during my graduate studies at Montana State University. Also I would like to thank N. R. Shivaparan for all his collaboration and continuous assistance. My thanks go to N. Williams and E. Andersen for their technical support and assistance.

This work was supported a grant by the National Science Foundation – Grant No. NSF Grant DMR - 9409205.

TABLE OF CONTENTS

1. Introduction **1**

2. Experimental Setup **3**

The Ultrahigh Vacuum Chamber 3

The Accelerator and Helium High Energy Particle Detector 5

The X-ray Photoelectron Spectrometer 6

The Reverse View Low Energy Electron Diffraction Optics 8

3. Experimental Techniques **11**

Sample Preparation 11

High Energy Ion Scattering 13

X-Ray Photoelectron Diffraction 15

X-Ray Photoelectron Spectroscopy 15

Experimental Design 17

Single Scattering Theory 18

Low Energy Electron Diffraction 20

4. Experimental Results for the Deposition of Ultrathin Ti Films on Al(110) **31**

Rutherford Backscattering 31

X-Ray Photoelectron Diffraction 31

Curve Fitting 31

Results 34

Low Energy Electron Diffraction 41

5. Interpretation of the Results **46**

X-Ray Photoelectron Diffraction Results 46

Low Energy Electron Diffraction Results 51

6. Conclusion **63**

BIBLIOGRAPHY **64**

LIST OF FIGURES

1 Schematic side view of the chamber 4
2 Schematic top view of the chamber 5
3 X-ray photoelectron spectroscopy system 7
4 Schematic diagram of the LEED optics and electrical connections . . 10
5 XPS spectrum of the Al 2p peak for (a) before sputtering and (b) after sputtering showing the clean crystal. 22
6 RBS spectrum for an 8.9 ML thick Ti overlayer on Al 23
7 XPS spectrum of Ti. The Ti 2p core-level peak is split due to spin-orbit interaction. 24
8 Geometry of the XPD experiment 25
9 Schematic representation of the XPD experiment 26
10 Scattering amplitude for an electron plane wave incident on a Cu atom at different energies [9] 27
11 Structural diagram illustrating the interplanar distortion that can be achieved by pseudomorhic growth. 28
12 Defocusing effect. The first one or two scattering events tend to be forward-focusing and subsequent events tend to be defocusing. 29
13 Relation between the LEED diffraction pattern and the reciprocal k *space* 30
14 XPS peaks for Al ($2p$) and Ti ($2p_{\frac{1}{2}}$ and $2p_{\frac{3}{2}}$). The dotted line represents the background. The peak areas after background subtraction are shown below the actual peaks. 33
15 XPD pattern for Al(110) secondary electrons. The figure shows the polar angle dependence of the background and the spline fit through the background. 35
16 *fcc* crystal direction and respective angles for the [110] and [100] azimuths 36
17 Polar angle scans of the Al 2p peak area in the [110] substrate azimuth for different coverages of Ti on Al (110) 37
18 Polar angle scans of the Al 2p peak area in the [100] substrate azimuth for different coverages of Ti on Al(110) 38
19 Polar angle scans of the Ti $2p_{\frac{1}{2}}$, $2p_{\frac{3}{2}}$ combined peak area in the [110] substrate azimuth for different coverages of Ti on Al(110) 39
20 Polar angle scans of the Ti $2p_{\frac{1}{2}}$, $2p_{\frac{3}{2}}$ combined peak area in the [100] substrate azimuth for different coverages of Ti on Al(110) 40
21 LEED patterns for Al with different coverages of Ti. (a) - (c) show the LEED patterns for energies 46.8 eV, 48.9 eV, and 46.8 eV for clean Al and two different coverages of Ti. (a) clean Al, (b) 1.9 ML of Ti on Al, (c) 5.5 ML of Ti. 42
22 LEED patterns for Al with different coverages of Ti. (a) - (d) show the spots for energies 86.2 eV, 90.4 eV, 86 eV, and 119 eV for clean Al and three different coverages of Ti. (a) clean Al, (b) 1.9 ML of Ti on Al, (c) 5.5 ML of Ti, (d) 8.1 ML of Ti. 43
23 Identification of the LEED spots for 46 eV and 86 eV and the angle between the two axis for clean Al and coverages of 1.9 ML and 5.5 ML. 45
24 Polar angle distribution of the Al $2p$ intensity for clean Al and with a coverage of 1.8 ML of Ti on Al(110) in the [110] azimuth 54
25 Polar angle distribution of the Al $2p$ intensity for Al for 4.8 ML and 8.9 ML coverages of Ti in the [110] azimuth 55

26 Polar scan for the Ti 2*p* for a coverage of 1.8 ML of Ti on Al(110) in the [110] azimuth. 56

27 Comparison between the Ti polar scan for 1.8 ML and the Al scan for clean Al in the [110] azimuth. 57

28 Polar scan for the Ti 2*p* for a coverage of 1.8, 2.5, and 4.8 ML of Ti on Al(110) in the [110] azimuth. 58

29 *fcc* lattice structure indicating a change due to strain 59

30 Polar angle scans for Al and Ti in the [110] azimuth. The diffraction pattern for Ti is taken for 8.9 ML of Ti on Al. The Al pattern is shifted to allow a better comparison. 60

31 Mechanism of the lattice distortion that can cause the observed LEED patterns. 61

32 Distortion of the LEED spots. Indicated are the changes in angles and distances. 62

LIST OF TABLES

1 Deposition Parameters and resulting thicknesses 32

2 Angles and distances for LEED spots 44

ABSTRACT

The growth of Ti films on the Al(110) surface at room temperature has been studied using X-ray photoelectron diffraction (XPD) and low energy electron diffraction (LEED). The overlayer coverages were determined with RBS. The area under the Al $2p$ and the Ti $2p\frac{1}{2}$ and $2p\frac{3}{2}$ photoelectron peaks was recorded in dependence of the polar angle.

Both LEED and XPD support an epitaxial growth of Ti on Al in form of islands. The structure of the Ti overlayer is pseudomorphic *fcc*. A distortion of the overlayer was measured with LEED. The interlayer distance of the first two Ti overlayer is smaller than that for the bulk Al as can be concluded from a shift of the forward-scattering peak in the diffraction pattern for Ti.

A shift of the forward-scattering peak in the polar angle scan for Al indicates an expansion of the first top layers in the Al substrate. Due to the absence of a strong forward-scattering peak in the Al scan for coverages above three monolayers the interdiffusion of bulk Al into the Ti film can be ruled out.

The Ti overlayer exhibits no long-range order for coverages of eight monolayers but still shows short-range order according to XPD.

CHAPTER 1

Introduction

For the development of state-of-the-art electronic device technology the growth of ultrathin epitaxial films on single-crystal substrates becomes more and more important. The growth of epitaxial films and the formation of metastable phases of the overlayer material lead to new directions in the search for new materials. These phases are occasionally the result of lattice mismatches which lead to a structure that is different from the equilibrium one at room temperature.

For example, face-centered cubic (*fcc*) Co films grow epitaxially on Cu(001) substrates [1], [2]. Both Al and Au can in principle grow epitaxially on GaAs(001) by nucleating an *fcc* overlayer in which the surface unit mesh of the overlayer is rotated by 45° with respect to that of the substrate [4].

Saleh and coworkers as well as Jona et.al. previously studied the growth of thin Ti films on Al(110) and Al(100) surfaces [6], [21]. Thin Ti films are of considerable interest for their application as diffusion barriers in semiconductors. The main conclusion of the work by Saleh et.al. was that Ti deposition on Al(110) results in the formation of an epitaxial Ti overlayer. A critical thickness of this metastable overlayer is reached for approximately 5 monolayers (ML) as reported by Saleh [6]. Saleh showed that the Ti adopts the surface symmetry and lattice constant of the underlying Al and forms an *fcc* overlayer. This is particularly interesting since the *fcc* structure of Ti does not occur in the equilibrium phase diagram of Ti at any temperature [3]. Saleh further concludes using the VEGAS-simulation of shadowing of the Al atoms by overlaying Ti atoms that the Ti does not form islands.

The situation for coverages exceeding 5 ML is not clear however. Two different growth modes are suggested: Island formation for Ti coverages above 5 ML and interdiffusion of Ti and Al atoms at the interface.

The present study examines the growth of Ti films on Al(110) surfaces using X-ray photoelectron diffraction (XPD) to supplement the results by Saleh. XPD is well suited to the study of the structure of very thin transition-metal films, because XPD diffraction patterns are collected from each chemical species in the sample independently. These patterns arise primarily from the local structure of a few atomic shells surrounding the emitting atom, so that long-range order is not necessary.

Through XPD we hope to gain an even better understanding of the epitaxial growth of Ti on the Al(110) surface. Ti films of up to 9 ML were deposited on the Al single crystal and the atomic structure of both the overlayer and the substrate were studied *in situ*. XPD measurements were done for clean Al and at coverages of 1.8 ML, 2.5 ML, 4.8 ML and 8.9 ML of Ti. A separate set of LEED experiments were carried out at 1.9 ML, 5.5 ML, and 8.1 ML coverages of Ti.

CHAPTER 2

Experimental Setup

A very clean surface free of contaminants is necessary for conducting experiments that involve surface phenomena. The experiments were therefore carried out in an ultrahigh vacuum chamber.

In our study the chamber is connected to a VAN DE GRAAF accelerator allowing the use of RUTHERFORD backscattering to determine the thickness of the deposited layer. Furthermore the chamber is equipped with an X-ray photoelectron spectroscopy system to do X-ray photoelectron diffraction and with reverse view low energy electron diffraction (LEED) optics for LEED analysis.

The present chapter gives an overview of the system and the experimental setup.

The Ultrahigh Vacuum Chamber

All experiments were performed in an ultrahigh vacuum (UHV) chamber. The use of such a vacuum chamber is crucial for the investigation of surface phenomena because it minimizes contamination of the sample. At pressures below 10^{-10} *Torr* (UHV environment) it takes several hours for the sample surface to become contaminated by the adsorption of residual gas atoms. In addition, UHV environments are beneficial for all ion- and electron-based surface analytical techniques, because the mean-free-path of electrons and ions is very short at atmospheric pressure.

Schematic views of the chamber and its components are shown in Figures 1 and 2. The UHV chamber is made of stainless steel and the inside is lined with *mu metal*

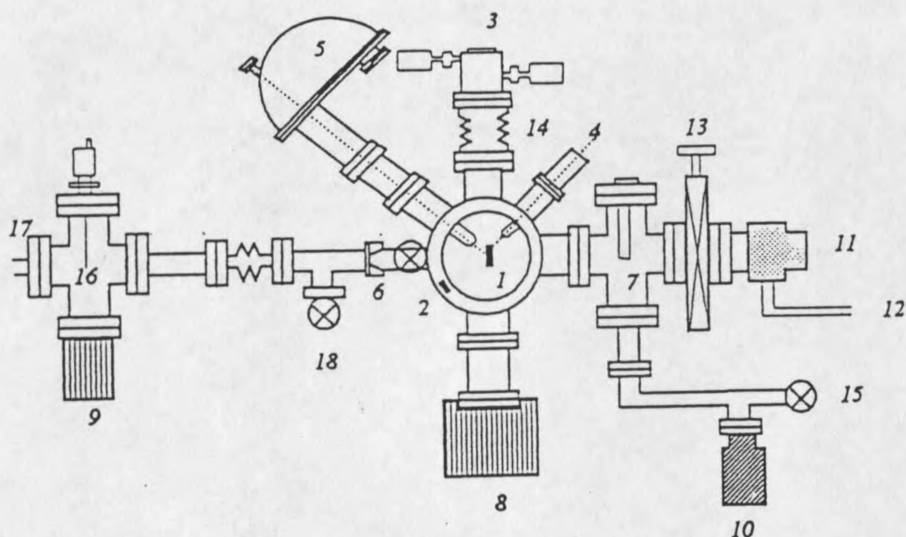

Figure 1: Schematic side view of the chamber

1. Sample
2. Detector
3. Goniometer
4. Sputter Gun
5. Hemispherical Analyzer
6. Collimator Slits
7. Ti sublimation pump
8. Ion Pump
9. Ion Pump
10. Sorption Pump
11. Turbo Pump
12. Foreline Pump
13. Gate Valve
14. Bellows
15. Leak Valve
16. Beam Blocker
17. Ion Beam Line
18. Valves

to provide magnetic shielding.

The chamber is equipped with a turbomolecular pump (*Balzers TPU 160*), an ion getter pump (*Varian*), and a titanium sublimation pump. To reach a regime in which the UHV pumps are operable a roughing pump with a foreline trap is connected to the chamber through the turbomolecular pump. An ionization gage and a quadrupole residual gas analyzer (*Dycor Electronics M100M*) are mounted to the chamber to monitor the pressure as well as the gas composition in the chamber. A pressure in the low 10^{-10} $Torr$ range is obtained by baking the chamber at 150^0C for about 48